# Development of an X-Ray Radiography Platform to Study Laser-Direct-Drive Energy Coupling at the National Ignition Facility

L. Ceurvorst,[1] W. Theobald,[1,2] M. J. Rosenberg,[1] P. B. Radha,[1] C. Stoeckl,[1] R. Betti,[1,2] K. S. Anderson,[1] J. A. Marozas,[1] V. N. Goncharov,[1,2] E. M. Campbell,[1] C. M. Shuldberg,[3] R. W. Luo,[3] W. Sweet,[3] L. Aghaian,[3] L. Carlson,[3] B. Bachmann,[4] T. Döppner,[4] M. Hohenberger,[4] K. Glize,[5] R. H. H. Scott,[5] A. Colaïtis,[6] and S. P. Regan[1,2]

[1]Laboratory for Laser Energetics, University of Rochester
[2]Department of Mechanical Engineering, University of Rochester
[3]General Atomics
[4]Lawrence Livermore National Laboratory
[5]Central Laser Facility, STFC Rutherford Appleton Laboratory
[6]Centre Lasers Intenses et Applications, Université de Bordeaux-CNRS-CEA

The coupling of laser energy to an imploding target in direct-drive inertial confinement fusion (ICF) is a key parameter that determines the ablation pressure and the implosion velocity of the shell. According to current models, cross-beam energy transfer (CBET) is a major factor that limits the ablation pressure on National Ignition Facility (NIF)-scale targets, reducing implosion velocity and shell kinetic energy. Hence, accurate measurements of the laser coupling efficiency for NIF-scale implosions are an important aspect of direct-drive ICF research. To obtain these measurements, a platform was developed on the NIF using x-ray radiography and self-emission imaging to diagnose the evolution of a directly driven solid spherical target. This plastic (CH) sphere was driven by 184 NIF beams in polar direct drive at three different intensities using a 7-ns ramp pulse. The remaining eight NIF beams were focused onto a copper backlighting foil to generate x rays that probed the target before being collected by a pinhole array coupled to a gated x-ray detector. This summary details the analysis technique used to reconstruct the target's density profile from these radiographs.

In the paraxial approximation, where the x rays are roughly parallel to the optical axis, the transmission $T$ of x rays passing through a plasma is given by:

$$\begin{aligned} T(x,y) &= e^{-\tau(x,y)} \\ \tau(x,y) &= \int \mu(x,y,z)\rho(x,y,z)\mathrm{d}z, \end{aligned} \tag{1}$$

where $\tau$ is the optical depth, $\mu$ is the opacity, and $\rho$ is the density. The implosions performed in these experiments are expected to remain roughly spherically symmetric, meaning that both the opacity and density should primarily be radial functions. In this limit, Eq. (1) shows that the optical depth is simply the Abel transformation of the attenuation, equal to the opacity times the density. Therefore, the radiographs can be converted to optical depth images, azimuthally averaged, and Abel inverted to yield the attenuation profiles.

To convert radiographs to optical depth images, the transmission of the target must first be inferred by dividing the raw signal by a fitted backlighter profile. Typically, this is done by fitting the unobstructed portions of the backlighter emission with an appropriate function, in this case, the superposition of two super-Gaussians. As can be seen in Fig. 1(a), however, the backlighter was largely eclipsed by the target itself, leaving little unobstructed data with which to perform the fit. Instead, the entire image was used in the calculations by multiplying the backlighter emission profile by a simplified transmission function, resulting in fits such as the one shown in Fig. 1(b). The transmission images were then obtained by dividing the raw image by the fitted backlighter emission as displayed in Fig. 1(d).

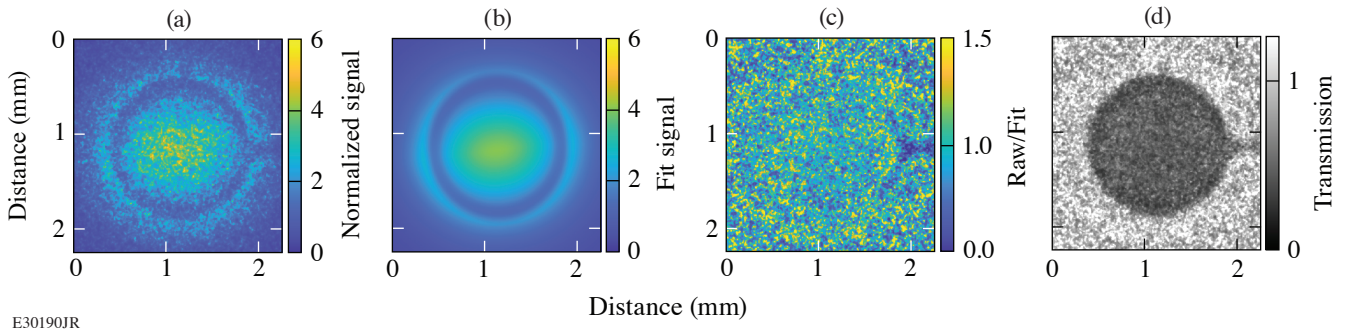


Figure 1
Converting radiographs into transmission images. (a) A single radiographic sub-image is taken from shot N210519-001 7.1 ns after the start of the drive. (b) This image is then fit with a simplified backlighter and transmission profile. (c) Dividing the raw radiograph by its fitted profile produces a flat image composed primarily of noise, confirming the quality of the fit. Note the stalk is not included in the fit and thus appears on the right side of this image. (d) The raw image is divided by the fitted backlighter profile to produce the final transmission image.

The resulting transmission was then converted to optical depth using Eq. (1), and the azimuthally averaged optical depth profiles were Abel inverted to obtain the system's radial attenuation. The final step of analysis was to separate the density and opacity profiles. Ahead of the shock, the target should not be significantly heated, maintaining its cold opacity value. After the shock, however, the material can be heated and ionized enough to reduce its overall opacity. A crude approximation was made that the opacity should be roughly constant in this shocked region, and its value was determined by matching the calculated target mass in the experiment to the accompanying *DRACO*[1] simulations. This yielded a hot opacity of 2.5±0.2 $cm^2/g$, similar to the 2.7 $cm^2/g$ calculated by post-processing the simulations with *Spect3D*.[2]

Using this step function for the opacity, the final density profiles were inferred and compared to the simulations as shown in Fig. 2. The shock trajectories were in rough agreement, indicated by the rise in density. However, the subsequent fall in density corresponding to the ablation front occurred at a larger radius in the experiment compared to the simulations. This is similar to the trends seen previously with thin-shell targets.[3] At the time, the thicker observed shocked region was suspected to be caused by hydrodynamic instabilities. However, the ablation front is not accelerating here, largely eliminating this possibility.

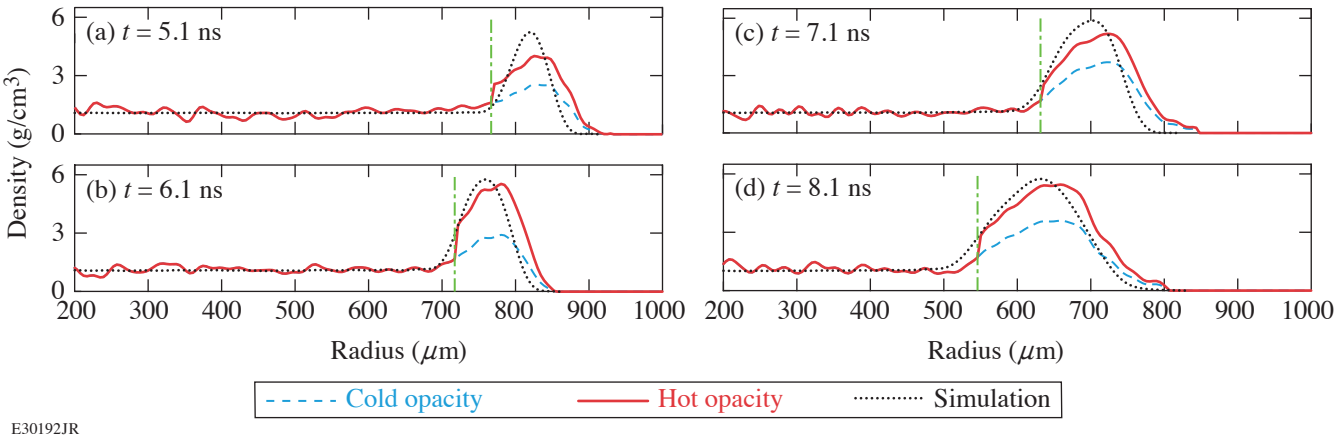


Figure 2
Inferred azimuthally averaged density profiles. The initial density calculation using only cold opacity (dashed blue curve) and mass conserving calculation using a stepped opacity profile (solid red curve) are compared to the simulated density profile convolved with the instrument response function of the system (dotted black curve) (a) 5.1 ns, (b) 6.1 ns, (c) 7.1 ns, and (d) 8.1 ns after the start of the drive. Vertical (dashed–dotted green) lines indicate the shock position beyond which the calculated hot opacity was applied.

To confirm that this discrepancy was not caused by the analysis technique, the same algorithm was applied to artificial radiographs calculated using *Spect3D*. The results of this analysis showed a 0.06 g/cm$^3$ rms error caused largely by the Abel inversion algorithm. As shown in Fig. 3, no shift to the reconstructed shock and ablation fronts was detected. The analysis also investigated the role of noise, which showed no systematic shift to these trajectories. The discrepancy in ablation front trajectory, therefore, appears to be physical. A comparison to simulations at all explored intensities and pulse shapes is now underway to distinguish between various effects such as preheat, CBET, and nonlocal heat-transport models. The results of this ongoing investigation will be published in a future manuscript.

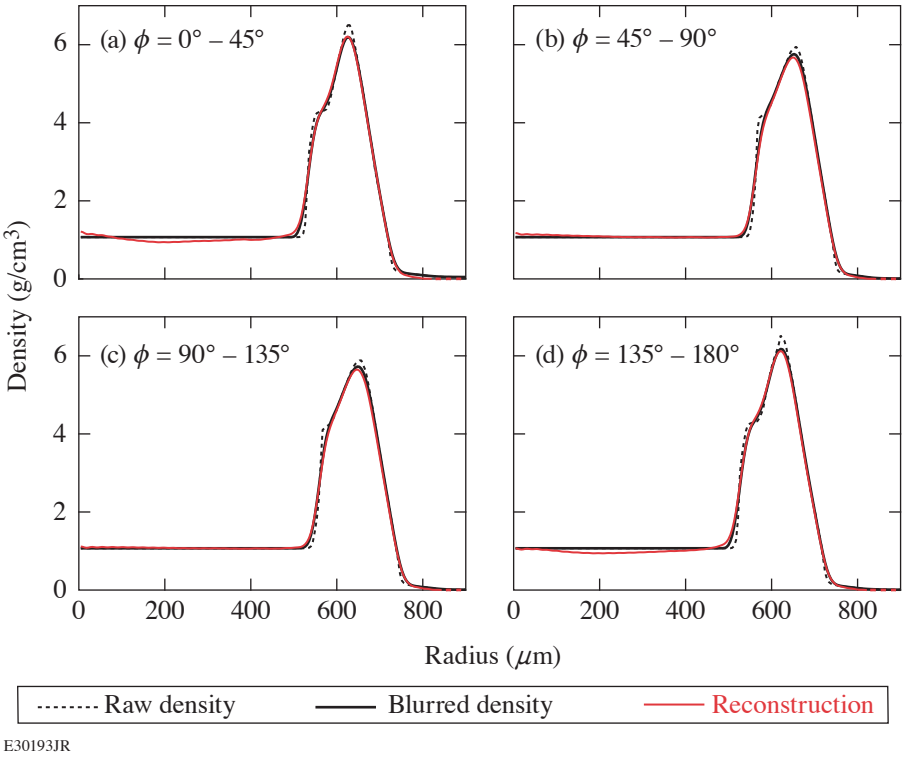


Figure 3
Validation of technique. Transmission images are calculated using *Spect3D*, and azimuthally dependent density profiles are reconstructed using this analysis technique. The data were calculated using azimuthal bins of (a) 0° to 45°, (b) 45° to 90°, (c) 90° to 135°, and (d) 135° to 180°. The reconstructed profiles (solid red curves) closely align with the original density profiles after accounting for the instrument response (solid black curves). The rms error between these two curves is 0.06 g/cm$^3$. Compared to the original density profile (dashed black curve), more features are lost because of imaging resolution than because of the reconstruction technique.

This material is based upon work supported by the Department of Energy National Nuclear Security Administration under Award Number DE-NA0003856, the University of Rochester, and the New York State Energy Research and Development Authority.

1. P. B. Radha *et al.*, Phys. Plasmas **23**, 056305 (2016).
2. J. MacFarlane *et al.*, High Energy Density Phys. **3**, 181 (2007).
3. M. Hohenberger *et al.*, Phys. Plasmas **22**, 056308 (2015).